JJEE

Volume 3, Number 1, 2017
Pages 1-18

Jordan Journal of Electrical Engineering

ISSN (Print): 2409-9600, ISSN (Online): 2409-9619

A Novel Approach for Parasitic Decoupling Element Design for MIMO Applications

Saqer S. Alja'afreh[1a], Yi Huang[2b], Lei Xing[3c], Qian Xu[3d]

[1]Department of Electrical Engineering, Mu'tah University, Al-Karak, Jordan
[2]Department of Electrical and Electronics Engineering, University of Liverpool, Liverpool, United Kingdom
[3]Department of Electronic and Information Engineering, Nanjing University of Aeronautics and Astronautics, Nanjing, China
[a]e-mail: saqer1981@yahoo.com
[b]e-mail: yi.huang@liv.ac.uk
[c]e-mail: xinglei@nuaa.edu.cn
[d]e-mail: emxu@foxmail.com

Received: October 19, 2016 *Accepted: December 22, 2016*

Abstract— Mutual coupling is a critical issue in the design of MIMO antennas as it deteriorates MIMO and diversity system performance. This work presents a novel approach and guideline for the design of a compact parasitic decoupling element between two element MIMO antennas. It is based on a stepped impedance resonator circuit theory, where the antenna impedance bandwidth, the level of isolation and compactness can all be controlled and optimized. Using this theory, a compact planar inverted-L dual-element antenna with a parasitic decoupling element is proposed for handset terminal applications. Measurement results show that this design has a good performance over the frequency range 1700-2700MHz, which covers most of cellular frequency bands, such as DCS 1800, PCS 1900, UMTS, and LTE-advanced between 1700-2700MHz. Finally, diversity performance parameters are obtained and evaluated based on both the simulated and measured results.

Keywords— Multiple input multiple output (MIMO), Mutual coupling, Planar inverted-L antenna (PILA), Parasitic decoupling element, Stepped impedance resonator (SIR).

I. INTRODUCTION

Over the last 25 years, mobile communications industry has enjoyed a rapid growth: it has evolved from 1G to digital 2G and from 3G to 4G systems now. The multiple-input and multiple-output (MIMO) technology has been introduced to improve both the system reliability and spectrum efficiency. However, placing multiple antennas into a small mobile terminal is very challenging; this is mainly due to the mutual coupling problem between closely spaced antennas. A strong mutual coupling means a high correlation between the signals antennas receive. The MIMO performance is based on: the antenna efficiency, channel capacity and diversity gain. Thus, decoupling antenna elements is a critical issue in MIMO technology and antenna diversity systems [1]. A lot of isolation (decoupling) techniques have been proposed in literature, which can be grouped into two broad categories:

1) Circuit level decoupling: This approach only needs knowledge about antenna impedances with no need to modify the antenna structure and ground plane. For example, a decoupling and matching network (DMN) is usually made by inserting a transmission line section (that realizes the complex conjugate matching for antenna impedances) between closely coupled antennas [2]-[4]. For the purpose of size reduction, this decoupling technique can be realized using lumped elements [5]. However, the usefulness of this technique can be limited by the size (the transmission line section) and low total efficiency which results from the Ohmic loss in the lumped elements [6]. Furthermore, this decoupling technique is considered as a narrow band solution that increases the detuning sensitivity of the antenna structure [7].

Corresponding author's e-mail: saqer1981@yahoo.com

2) Antenna level decoupling: This represents the decoupling techniques that require a modification on the antenna structure or ground plane. Several decoupling techniques fall under this category:

a) Defect ground plane structure (DGS): The surface current on the common ground plane can be altered by changing the ground plane. This modification can produce a band-stop filtering operation to achieve a high isolation level [8]. However, there are two possible drawbacks with DGS: a narrow bandwidth and hard to implement in reality as the ground plane is shared with other components.

b) Energy band gap structure (EBG): Another kind of modification can be done by using artificially periodic structures [9]. An EBG can suppress the surface wave between closely spaced antennas and provide a high isolation level; yet, it suffers from a narrow bandwidth of isolation, a large area and complicated structures.

c) Neutralization line: Adding a conducting strip between closely coupled antennas can provide a reverse coupling path that maintains the isolation. Although it has been widely reported in literature [10], [11], the design procedure of this neutralization line differs from the analytical formulation of the aforementioned techniques. This makes the final structure sub-optimal in term of the footprint, decoupling level and decoupling bandwidth [12].

d) Parasitic decoupling element: The possibility of inserting an additional distributed parasitic element has been explored in several projects [1], [13]-[16]. This solution is to add an additional coupling path between closely coupled antennas by the field cancelation [1]. Though this solution has little Ohmic loss and is very suitable for handset integration [12], there is no general design rule or procedure to obtain optimal results for a small footprint, wide isolation bandwidth and acceptable isolation level. Thus, a thorough investigation on the circuit theory is needed.

As the circuit theory is usually needed to complete the design cycle and offer better understanding of the distributed circuit characteristics, this paper presents a novel design approach for a parasitic decoupling element inserted between two coupled antennas. It is based on the stepped impedance resonator (SIR) circuit theory, which has the following features:

1) A small footprint decoupling element can be achieved;

2) It provides a wideband decoupling solution;

3) It offers a tradeoff between the decoupling bandwidth and isolation level;

4) It offers two functions for the parasitic element; it can work as either a decoupling element that enhances the isolation level or a decoupling and radiation element which enhances both the impedance bandwidth and the decoupling bandwidth.

As a design example, a wideband low profile dual-element PILA with a parasitic decoupling element is proposed for handset applications in the frequency range 1700-2700 MHz.
In this paper, section 2 introduces the theory of SIR and the general configuration of the equivalent coplanar waveguide (CPW) SIR structure. In section 3, a new antenna is designed, made and tested using the proposed design approach. In Section 4, the diversity performance parameters are obtained, evaluated and discussed. Finally, the conclusion is drawn in Section 5.

II. SIR THEORY AND THE PROPOSED DESIGN METHOD

A. SIR Theory

Fig. 1 shows a basic structure of a quarter-wavelength SIR. It represents a transmission line with two different characteristic impedances Z_1 and Z_2 and two different electrical lengths θ_1 and θ_2, respectively.

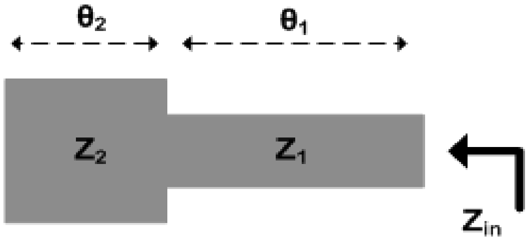

Fig. 1. Layout of a conventional two-section quarter wavelength SIR

As the structure represents an open circuit transmission line (from Z_2 end), the resonance condition for any odd multiple of quarter wavelength can be obtained when the input impedance is zero:

$$Z_{in} = jZ_1 \frac{Z_1 \tan(\theta_1)\tan(\theta_2) - Z_2}{Z_1 \tan(\theta_2) + Z_2 \tan(\theta_1)} = jZ_1 \frac{\tan(\theta_1)\tan(\theta_2) - R_z}{\tan(\theta_2) + R_z \tan(\theta_1)} = 0 \quad (1)$$

Yielding the resonance condition as follows:

$$\tan(\theta_1)\tan(\theta_2) - R_z = 0 \Rightarrow R_z = \frac{Z_2}{Z_1} = \tan(\theta_1)\tan(\theta_2) \quad (2)$$

where R_z is the impedance ratio Z_2/Z_1.

The above resonance condition shows that SIR resonance frequency can be controlled by more than one design parameter; both electrical length and impedance ratio play important roles in determining the resonance frequency of SIR [17]. Furthermore, one interesting property of SIR over the uniform impedance resonator (UIR) is compactness; SIR can have a minimum length at the same resonance frequency when the impedance ratio $R_z<1$; it can have a maximum length when $R_z>1$ [17]-[19].

In order to enhance the resonator bandwidth and achieve a more compact design, a multi-step resonator is usually employed over a two-step resonator. As an example, a three-step SIR is created in Fig. 2. A new section with characteristic impedance Z_3 and electrical length θ_3 is inserted between the original sections 1 and 2. Similar to the analysis of a two-section SIR, the resonance condition of a three-section SIR can be drawn after letting the input impedance be zero. For the simplicity of both design and analysis, let the three sections have the same electrical length θ.

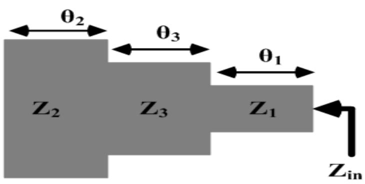

Fig. 2. Layout of tri-section quarter wavelength SIR

$$Z_{in} = jZ_1 \frac{Z_3^2\tan^2(\theta) - Z_2Z_3 + Z_1Z_3\tan^2(\theta) + Z_1Z_2\tan^2(\theta)}{Z_1Z_3\tan(\theta) + Z_1Z_2\tan(\theta) - Z_3^2\tan^3(\theta) + Z_2Z_3\tan(\theta)} = 0 \tag{3}$$

Let the impedance ratios be

$$K_1 = \frac{Z_2}{Z_3}, \; K_2 = \frac{Z_3}{Z_1} \tag{4}$$

Then, the resonance condition is:

$$\theta = \tan^{-1}\left(\sqrt{\frac{K_1K_2}{1+K_1+K_2}}\right) \tag{5}$$

Equation (5) can be further simplified using (4) and (2) as:

$$\theta = \tan^{-1}\left(\sqrt{\frac{R_z}{1+K_1+K_2}}\right) \tag{6}$$

For the case of two-section SIR with equal length, using (2), we have:

$$\theta = \tan^{-1}\left(\sqrt{R_z}\right) \tag{7}$$

It can be seen that the argument in (6) is scaled by $(1+K_1+K_2)^{1/2}$ which makes the multi-section SIR more compact than the two-section SIR.

B. Proposed Design Method

Fig. 3 represents a general geometry of dual-element monopole antenna with a parasitic decoupling element. For simplicity, the decoupling element is symmetrical between antennas. Referring to the transmission line theory and SIR theory, one can see the following: 1) the general configuration of the structure is similar to the configuration of transmission line stop band filter. The decoupling element represents an open circuit electrically coupled shunt stub (a shunt series LC resonator). This stub (decoupling element) represents a centre strip of coplanar waveguide (CPW) while the antenna elements act as the CPW ground strips. 2) The shape of the decoupling element shows that this stop band resonator is a kind of SIR stop band resonator (two-section SIR). From the aforementioned SIR theory, the stop band resonant frequency, isolation level and isolation bandwidth can be tuned by changing the characteristic impedance ratio between sections. This can be done by changing the widths (W_1 and W_2) and the gaps (g_1 and g_2) without increasing the total length of the decoupling element. More information about the design of CPW characteristic impedance and the effects of the width and gap parameters can be found in [20]. Using this theory, a compact parasitic decoupling element can be found with wideband isolation characteristics.

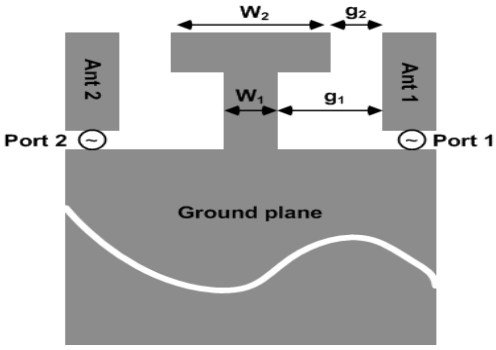

Fig. 3. General geometry of dual-element monopole antenna with a parasitic decoupling element

III. DESIGN EXAMPLE

A. Antenna Configuration and Scattering Parameters

A proposed mobile antenna is depicted in Fig. 4. The antenna includes two symmetrically modified- planar inverted-L antenna (PILA) elements [21]. Unlike [21], to save more space and to validate the proposed approach, both PILA elements are installed on the same PCB edge (upper edge). The top plate with dimensions of 5×15mm^2 is placed 5mm above the ground plane with an FR-4 substrate of dimensions 55×100×1.5mm^3, relative permittivity of ε_r=4.3 and a loss tangent of tan δ=0.025. Each antenna element is fed by a feeding strip of dimensions 2×5mm^2. To reduce the electrical length of each element, both capacitive loading (bending) and inductive loading (meandering) are employed by creating a vertically bended plate of dimensions 5×9mm^2. To enhance the radiation resistance, the ground plane is partially removed underneath the top plate; the dimensions of the ground free area are 7×55mm^2. All these dimensions are optimised via computer simulations. In order to reduce mutual coupling between the two elements, a parasitic decoupling element is added, designed and optimized based on the proposed approach. The design and optimization processes are presented in the next section. The decoupling element is located right in the middle of the two elements. It represents a three-section SIR band stop filter; the length of each section is 6.5mm while the widths are 1mm, 3mm and 23mm, respectively.

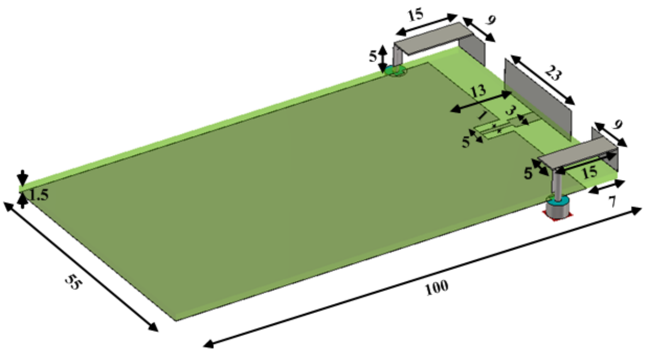

Fig. 4. Proposed dual-element antenna with dimensions in millimetres

The simulated scattering parameters are depicted in Fig. 5; and for comparison, the simulated performance without the parasitic decoupling element is added to Fig. 5. By adding the parasitic decoupling element, the mutual coupling is improved: S_{21} is decreased from -6dB to less than -12dB. Since the design has a dual resonance, the first one is linked to the parasitic element while the second one refers to antenna element; the -6dB S_{11} bandwidth is increased from about 1700-2800 MHz to 1700-3500 MHz.

To validate the proposed design, a prototype is fabricated and presented in Fig. 6. The measured S-parameters are depicted in Fig. 7. It can be observed that the measured results are very similar to the simulated ones in Fig. 5, and exhibit almost the same behaviour.

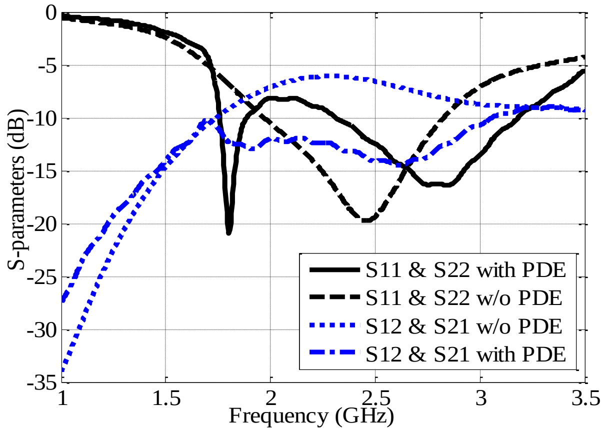

Fig. 5. Simulated scattering parameters (PDE: means parasitic decoupling element)

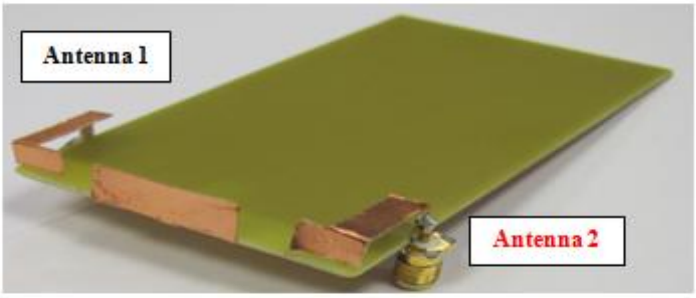

a)

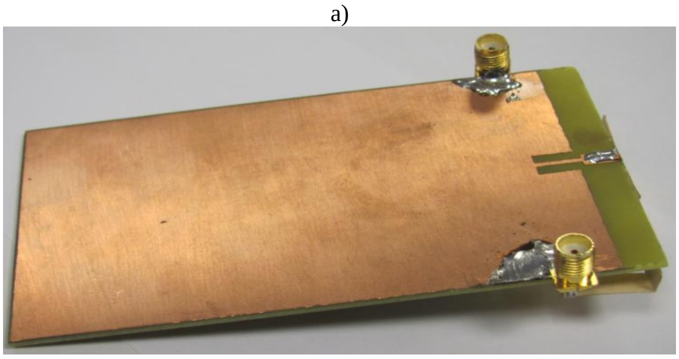

b)

Fig. 6. Prototype of the proposed antenna: a) top view and b) back view

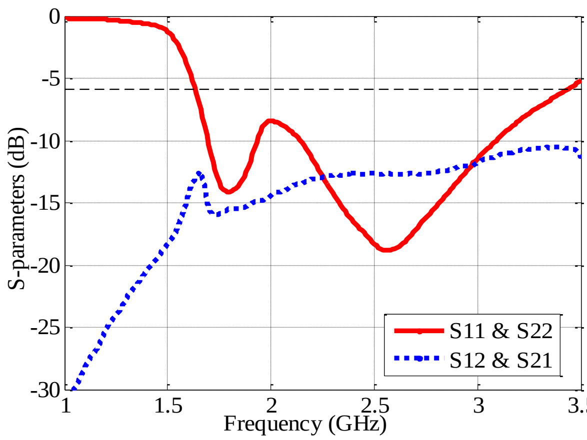

Fig. 7. Measured scattering parameters

B. Decoupling Element Design Approach

In this section, we are going to discuss the design steps for the decoupling element and its SIR band stop filter.

B.1. SIR Equivalent Structure

Referring to Fig. 8a, it can be seen that the decoupling element represents a three-section CPW SIR Structure, Fig. 8b shows the equivalent CPW for each section. Thus, the decoupling element represents a parallel coupled quarter wavelength SIR between antenna feeds. In order to use the SIR theory, the calculation of the characteristic impedance for each SIR section is needed; this requires a calculation of the effective permittivity.

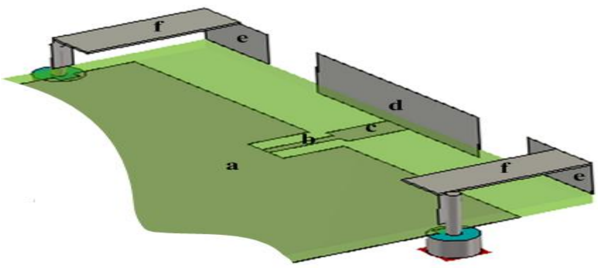

a)

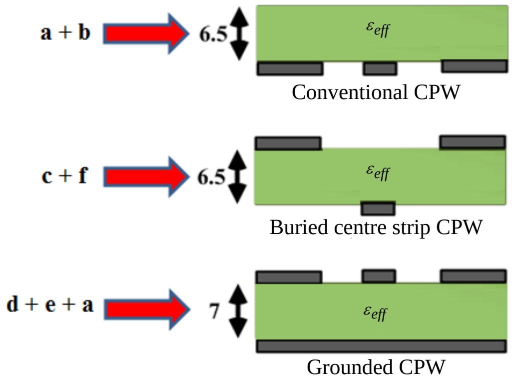

b)

Fig. 8. Equivalent CPWs from the proposed structure: a) proposed structure and b) the equivalent CPW schemes

B.2. Calculation of the Effective Permittivity

As the proposed structure represents a parallel plate capacitor (parallel antenna feeds) filled with two dielectric layers (vacuum and FR-4) parallel to the normal direction of the parallel plates as shown in Fig. 9a, the effective permittivity of the equivalent layer can be calculated based on the following relation [22]:

$$\varepsilon_{eff} = \sum_{i=1}^{N} \rho_i \varepsilon_i \qquad (8)$$

where ρ_i and ε_i represent the volume density and relative permittivity of the i_{th} layer respectively.

The question, which may arise now is how accurate this calculation is. Fig. 9b gives a clear answer where the S-parameter results in both cases are about the same (the original structure with FR-4 substrate and the case with the equivalent layer with effective relative permittivity equal to 1.75). This effective permittivity represents the permittivity of the equivalent layer in CPW schemes in Fig. 8b; and it is used for the calculations of characteristic impedance for each SIR section.

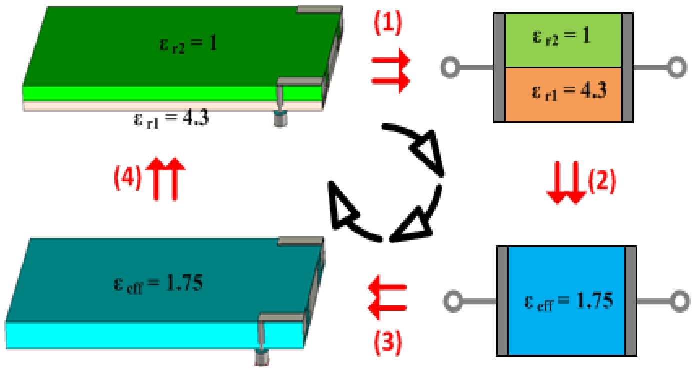

a)

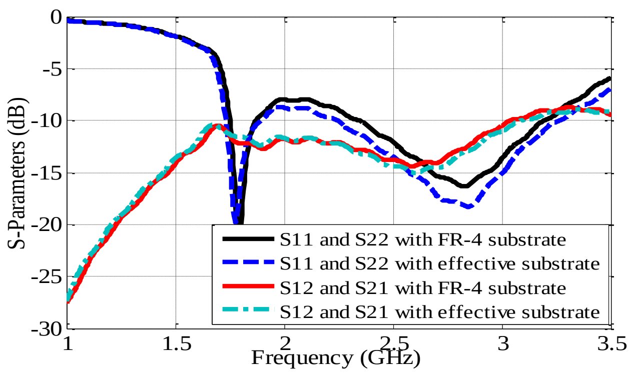

b)

Fig. 9. Effective permittivity: a) Parallel capacitance theory and b) Validation of the calculation

B.3. Two-Section SIR

Creating only one discontinuity on the decoupling element represents a two-section SIR structure formed from two coplanar waveguides: the first section represents conventional CPW with characteristic impedance Z_1 while the second section represents a grounded CPW with characteristic impedance Z_2 [23]. Fig. 10 and 11 show the effects of changing Z_1 and Z_2 on the level of the mutual coupling and the stop-band bandwidth, respectively. The total length of SIR has been kept constant. It can be seen that the mutual coupling impedance curve has a similar behaviour to the input impedance of the two-section SIR shown in (1).

Furthermore, the most important point which can be concluded from both figures is that: as the impedance ratio decreases, the stop band frequency moves downwards. In addition, Fig. 12 shows the effect of tuning the impedance ratio on the operational bandwidth. It can be seen that the operational bandwidth can be enlarged from the upper edge when the impedance ratio goes high. For a low ratio, it is enlarged from the lower edge frequency. This leads to the conclusion that the decoupling element works as a decoupling and parasitic element. Compactness can be achieved when the impedance ratio is low.

Table 1 summarizes the SIR analysis from simulation and theoretical point of views: it can be seen that the values of simulated resonance frequencies are in a good agreement with the theoretical values obtained using (1). In the analysis, CPW line structure is employed; the discontinuities in the step junctions and changes of the effective dielectric constant due to width and gap variations are all considered.

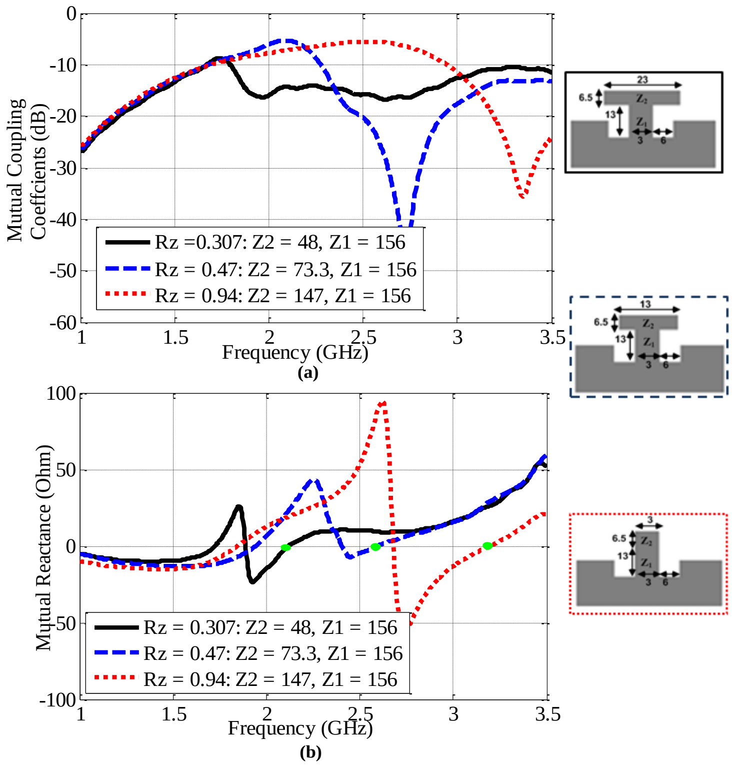

Fig. 10. Effect of changing Z_2: a) mutual coupling coefficient and b) mutual coupling impedance

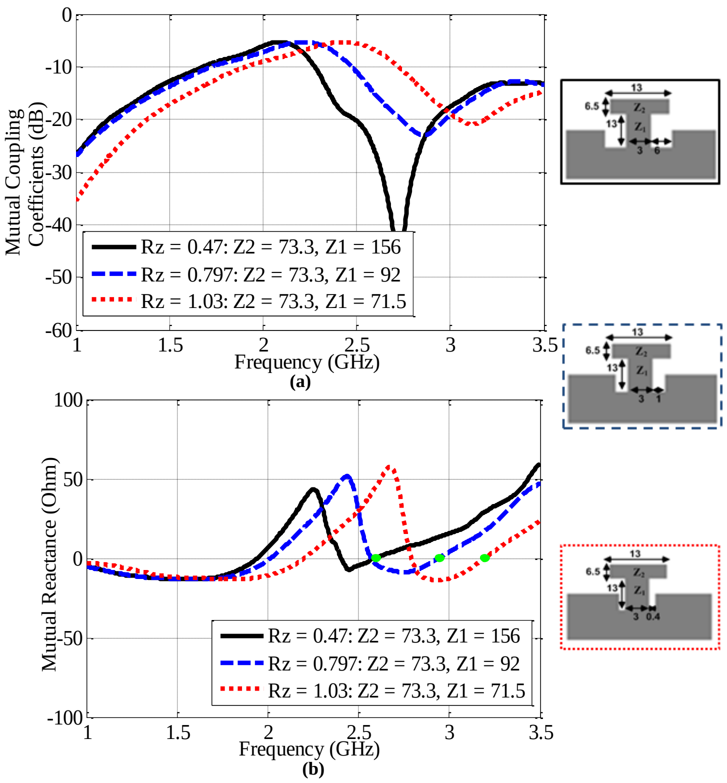

Fig. 11. Effect of changing Z_1: a) mutual coupling coefficient and b) mutual coupling impedance

TABLE 1
SUMMARY OF TWO SECTIONS SIR

Z_1, Ω	Z_2, Ω	ε_{e1}	ε_{e2}	R_z	f_z Simulated, GHz	f_z Theory, GHz
156	48	1.38	1.525	0.307	2.1	2.14
156	73.3	1.38	1.52	0.47	2.57	2.53
92	73.3	1.384	1.52	0.797	2.93	3.02
156	148	1.38	1.47	0.95	3.15	3.2
71.5	73.3	1.388	1.52	1.03	3.22	3.26

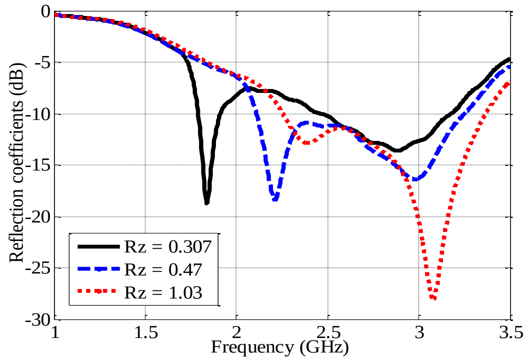

Fig. 12. Effect of changing impedance ratio on the reflection coefficients

B.4. Three-Section SIR

From the two-section SIR analysis, it can be seen that the level of mutual coupling around 1.7 GHz is quite high (Z_2= 48Ω and Z_1= 156Ω). To reduce this level, there are two possible solutions; the first one, which is not preferable, is to increase the length or width of the gap between the ground plane and Section 1 in the decoupling element; the second one, which is preferable, is to upgrade the two-section SIR into three-section SIR by creating two width discontinuities. By deploying the second solution, the total length of the decoupling element remains the same; and the ground plane gap around Section 1 gets small. Both the decoupling element and antenna elements can have a small footprint over the PCB (55mm×13mm). Fig. 13a shows the three equal lengths of the SIR; the first section is equivalent to the conventional CPW. The second section represents a buried CPW while the third section represents a grounded CPW [20]. The equivalent characteristic impedance for each of the three sections is Z_1= 156Ω, Z_2= 212Ω, Z_3= 48Ω, respectively. By substituting these values in (4) and (5), the resonance frequency of this structure is found to be 2.0GHz. The simulation result obtained using CST Microwave Studio has also verified this calculation as shown from the mutual impedance curve in Fig. 13c: the simulated stop-band resonance frequency is also around 2.0GHz. Furthermore, another advantage of using the three-section SIR shown in Fig. 13b is that the level of mutual coupling around 1.7GHz decreases to lower than -12dB. Table 2 compares the total electrical lengths for the two-section and three-section SIRs; it shows that the design with three-section is more compact than the two-section case. It is worth mentioning that during the calculation, the changes of the effective dielectric constant due to width and gap variations have been considered.

TABLE 2
TOTAL ELECTRICAL LENGTH COMPARISON

	Two-Section SIR	Three-Section SIR
Resonance Frequency, GHz	2.1	2.0
Total Electrical Length, rad	$\theta_1 + \theta_2 = 1.03$	$3\theta = 3(0.3) = 0.9$

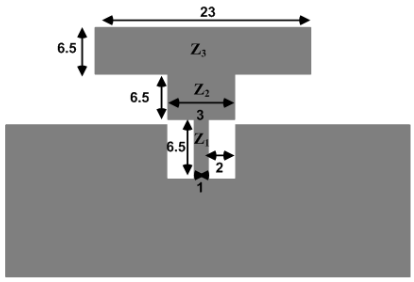

a)

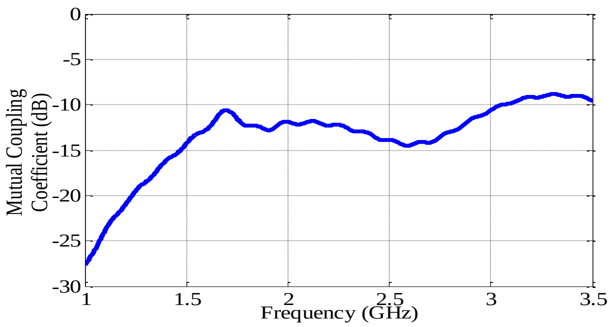

b)

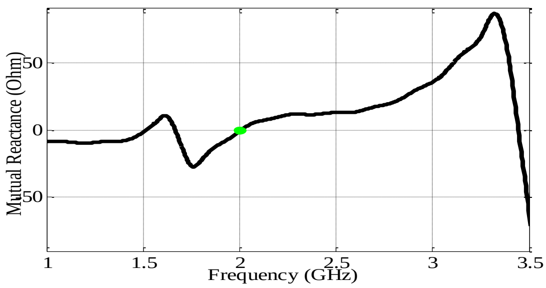

c)

Fig. 13. Three sections SIR: a) Structure, b) mutual coupling coefficient and c) mutual coupling impedance

IV. DIVERSITY PERFORMANCE

The diversity characteristics and MIMO performance of the dual-element antenna are simulated, measured and calculated in free space; important parameters like envelope correlation coefficient (ECC), mean effective gain (MEG) ratio, radiation patterns, total radiation efficiency and diversity are presented in this section.

A. Mean Effective Gain and Envelope Correlation Coefficient

Both MEG ratio and ECC represent the main diversity conditions [24]. The ECC is a measure of the difference in the received signals by the two elements, while MEG ratio is a measure of the power balance at the input ports of the two element antennas. The critical limits for both conditions are summarized as follows [24]:

$$\rho_e \leq 0.5 \text{ and } \left|\frac{MEG_1}{MEG_2}\right| \cong 0dB \tag{9}$$

where ρ_e is the ECC; k is the branch power ratio; and MEG is the mean effective gain.
The ECC can be calculated by different methods: using S-parameters [25] (accurate and fast for the case of loss free antenna in free space), using far field method [24] which is more accurate, or using the accurate S-parameters approach in [26] in which the antenna radiation efficiency is taken into account. On the other hand, the calculation of MEG ratio is mainly based on the radiation power pattern, total antenna efficiency and propagation characteristics of the mobile communication environment [27].
Experimentally, the calculation of both ECC and MEG ratio using integral approaches in [24], [27] is time consuming as it needs a 3D radiation pattern (which is also hard to obtain accurately in practice). Thus, the measured ECC is evaluated using the accurate S-parameter approach [26]. Fig. 14 shows a good agreement between the measured and simulated results. Both values have met the ECC condition in which ECC is less than 0.2 over the interested frequency band. To quantify the second diversity condition (MEG ratio), several propagation scenarios have been discussed in [29], [30] based on real measured values and statistical models like Gaussian, Laplacian and uniform distribution models. By loading the statistical parameters of Gaussian indoor and outdoor propagation environments into CST Microwave Studio, the calculated values of the MEG ratio in both environments satisfy the second diversity condition (less than 3dB [24], [28]) as shown in Table 3.

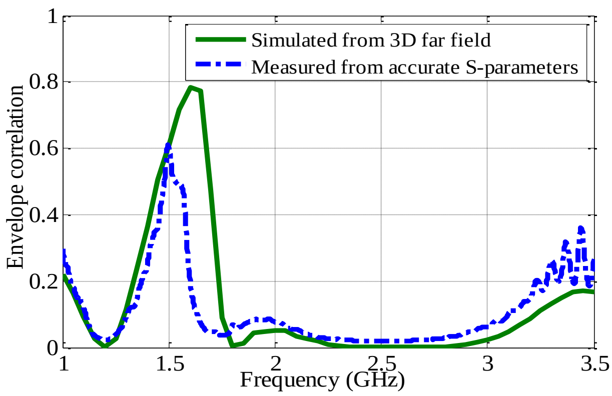

Fig. 14. Envelope correlation coefficient

TABLE 3
POWER BALANCE DIVERSITY CONDITION OVER DIFFERENT GAUSSIAN ENVIRONMENTS

Frequency, GHz	XPR, dB	MEG_1, dB	MEG_2, dB	$\|MEG_1\text{-}MEG_2\|$, dB
1.75	1	-3.02	-3.32	0.3
	6	-5.05	-5.36	0.31
2.7	1	-3.9	-3.7	0.2
	6	-6.45	-5.5	0.95

*Statistical parameters: m_V and m_H are mean elevation angles of the vertical and horizontal polarized wave distribution (Indoor m_H= m_V= 20°; Outdoor m_H= m_V= 10°), while σ_V and σ_H are the standard deviation of vertical and horizontal polarized wave distribution (Indoor σ_H= σ_V= 30; Outdoor σ_H= σ_V= 15) [29], [30].

B. Far-Field Radiation Patterns

The radiation pattern measurement was also conducted inside an anechoic chamber with one port excited and the other terminated to a 50 load. Fig. 15 shows the measured far field normalized patterns at two resonance frequencies 1.75 GHz and 2.7 GHz. The pattern diversity can be observed in both XY and XZ plane while, due to the symmetry of the structure, the radiation patterns in YZ plane look the same.

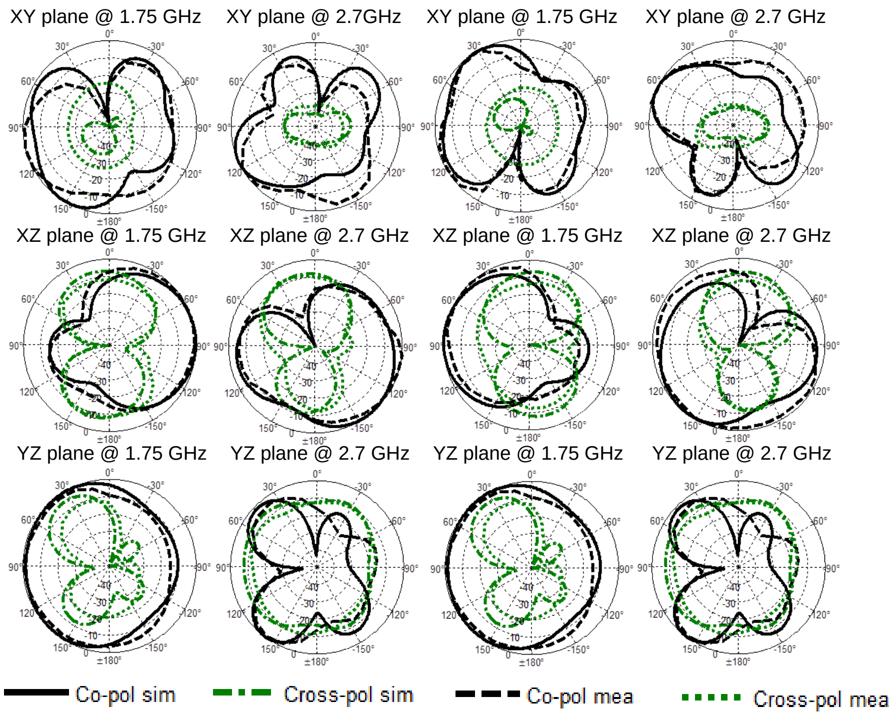

a) b)

Fig. 15. Measured and simulated normalized radiation patterns: a) Element 1 and b) Element 2

C. Measurement of Diversity Gain and Total Radiation Efficiency

The measurement process was conducted inside our reverberation chamber (RC), which is 3.6m×4m×5.8m in size. The measurement was performed in conjunction with a double ridged waveguide horn antenna (R&S®HF906) and a homemade PILA [31] with known radiation efficiency calculated via one-antenna approach inside the RC [31]. The reference antenna was connected to a VNA; and the scattering parameters were obtained over the frequency range 1-4GHz with 10,001 frequency sample points. The reason behind this large amount of sample points is to calculate the chamber decay time τ_{RC} from IFFT of S-parameters [32]. The need of τ_{RC} is to calculate the embedded radiation efficiency of AUT. The mechanical stirring sample number was 359 (1 degree/sample). Thus, in total 359×10,001= 3,590,359 samples were collected. For the reference antenna measurement, the AUT (antenna under test) was located inside RC; and both branches were terminated with 50Ω load. Once the reference measurement was completed, the same procedure was repeated for AUT branch 1 and branch 2, respectively. The reference antenna and unused branch are terminated with 50Ω loads. The diversity gain post-processing was carried out using a MATLAB programme. The main steps of the post-processing are stated in [33].

After calculating channel samples, the selection combining (SC) diversity scheme was applied; and the corresponding cumulative distribution function (CDF) for each channel was calculated. As the diversity gain is defined as the ratio of the output power of the diversity combiner to the power of the reference branch at a specified CDF probability level (usually 0.01), the apparent diversity gain @0.01 CDF depicted in Fig. 16 is about 10dB. This value is also verified from the measured ECC, which is about 9.75dB on average over the frequency band of interest.

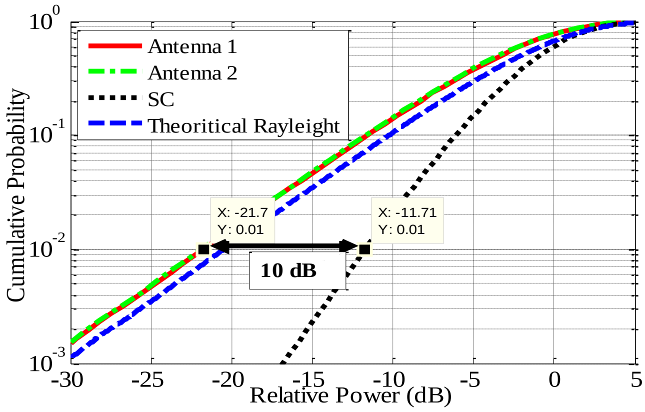

Fig. 16. CDF function and measured apparent diversity gain

As the design represents a multi-port antenna, it is important to calculate the total radiation efficiency using:

$$\eta_{Tot} = \eta_{rad}(1 - |S_{11}|^2 - |S_{12}|^2) \tag{10}$$

where η_{rad} is the radiation efficiency; S_{11} is the reflection coefficient of the antenna element; S_{12} is the transmission coefficient between two antenna elements.

The same collected data from the diversity gain measurement was used in calculating the total efficiencies. The simulated and measured total efficiencies are depicted in Fig. 17. It shows that the proposed antenna has a high total radiation efficiency (>80%) over the frequencies of interest.

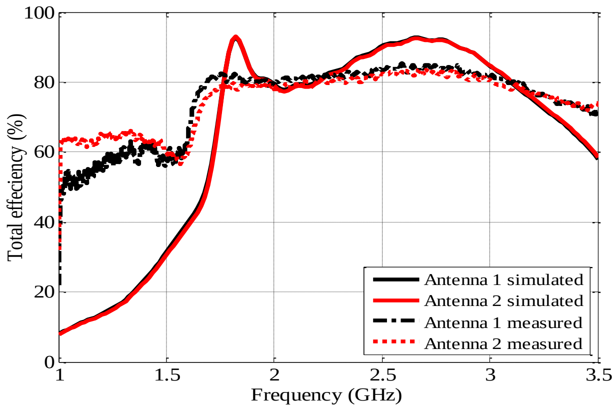

Fig. 17. Total radiation efficiency

V. DISCUSSION AND CONCLUSION

A new approach for designing a parasitic decoupling element between two-element MIMO antennas has been proposed in this paper. It offers some excellent features such as: 1) small footprint decoupling elements; 2) wide bandwidth; 3) controllability of the functionality of the decoupling element which can work as a decoupling element, parasitic radiator or both. Table 4 compares the total length of the proposed decoupling element with some recently published work; and it shows that the optimal size can be achieved by using this new approach.

As a MIMO antenna example, a low profile, small footprint and wideband dual-PILA-element antenna with a parasitic decoupling element has been presented for handset applications in the frequency range 1700-2700MHz. The calculated and measured results of the antenna have showed that it can be a very good candidate for MIMO and diversity systems. Moreover, the design is compatible with the recent handset antenna design industry trend (handset with metallic frame ID) as both the decoupling element and antenna element can be considered as a part of metal frame.

As a future work, since the neutralization line technique still lacks a design approach, we will employ the same design theory to find an optimal neutralization line structure in terms of the footprint, decoupling level and decoupling bandwidth.

TABLE 4
COMPARISON WITH PREVIOUS WORKS

Reference	Total Length	Lowest Frequency, GHz
[1]	$0.26\lambda_0$	2.4
[13]	$0.31\lambda_0$	1.92
[16]	$0.21\lambda_0$	2.4
This work	$0.18\lambda_0$	1.7

REFERENCES

[1] A. Mak, C. Rowell, and R. Murch, "Isolation enhancement between two closely packed antennas," *IEEE Transactions on Antennas and Propagation*, vol. 56, no. 11, pp. 3411-3419, 2008.

[2] J. Anderson and H. Rasmussen, "Decoupling and descattering networks for antennas," *IEEE Transactions on Antennas and Propagation*, vol. 24, no. 6, pp. 841-846, 1976.

[3] J. Wallace and M. Jensen, "Mutual coupling in MIMO wireless systems: a rigorous network theory analysis," *IEEE Transactions on Wireless Communications*, vol. 3, no. 4, pp. 1317-1325, 2004.

[4] L. Zhao, L. Yeung, and K. Wu, "A coupled resonator decoupling network for two-element compact antenna arrays in mobile terminals," *IEEE Transactions on Antennas and Propagation*, vol. 62, no. 5, pp. 2267-2276, 2014.

[5] S. Chen, Y. Wang, and S. Chung, "A decoubling technique for increasing the port isolation between two strongly coupled antennas," *IEEE Transactions on Antennas and Propagation*, vol. 56, no. 12, pp. 3650-3657, 2008.

[6] A. Sibille, C. Oestges, and A. Zanella, "Multiple antenna terminals," *in MIMO from Theory to Implemetation*, Academic Press, pp. 267-298, 2010.

[7] B. Lau, J. Anderson, G. Kristensson, and A. Molisch, "Impact of matching network on bandwidth of compact antenna arrays," *IEEE Transactions on Antennas and Propagation*, vol. 54, no. 11, pp. 3225-3238, 2006.

[8] C. Chi-Yuk, C. Chi-Ho, R. Murch, and C. Rowell, "Reduction of mutual coupling between closely-packed antenna elements," *IEEE Transactions on Antennas and Propagation*, vol. 55, no. 6, pp. 1732-1738, 2007.

[9] C. Chi-Yuk and Z. Du, "Microstrip antennas integrated with electromagnetic band gap EBG strucutures: a low mutual coupling design for array applications," *IEEE Transactions on Antennas and Propagation*, vol. 51, no. 10, pp. 2936-2946, 2003.

[10] A. Diallo, C. Luxey, P. Thuc, R. Staraj, and G. Kossiavas, "Enhanced two-antenna structures for universal mobile telecommunications system diversity terminals," *IET Microwaves, Antennas and Propagation*, vol. 2, no. 1, pp. 93-101, 2008.

[11] Y. Wang and Z. Du, "A wideband printed dual-antenna system with a novel neutralization line for mobile terminals," *IEEE Antennas and Propagation Letters*, vol. 12, pp. 1428-1431, 2013.

[12] M. Pelosi, M. Knudsen, and G. Pederson, "Multiple antenna systems with inherently decoupled radiators," *IEEE Transactions on Antennas and Propagation*, vol. 60, no. 2, pp. 503-515, Feb. 2012.

[13] Z. Li, Z. Du, M. Takahashi, K. Saito, and K. Ito, "Reduction mutual coupling of MIMO antennas with parasitic elements for mobile terminals," *IEEE Transactions on Antennas and Propagation*, vol. 60, no. 2, pp. 473-480, 2012.

[14] K. Payandehjoo and R. Abhari, "Investigation of parasitic elements for coupling reduction in multiantenna hand-set devices," *Rf and Microwave Computer-Aided Engineering*, vol. 24, no. 1, pp. 1-10, 2014.

[15] T. Wu, S. Fang, and K. Wong, "Printed diversity monopole antenna for WLAN operation," *Electronics Letters*, vol. 38, no. 25, pp. 1625-1626, 2002.

[16] G. Chi, B. Li, and D. Qi, "Dual-band printed diversity antenna for 2.4/5.2- GHz WLAN application," *Microwave and Optical Technology Letters*, vol. 45, no. 6, pp. 561-563, 2005.

[17] M. Sagawa, M. Makimoto, and S. Yamashita, "Geometrical structures and fundamental characteristics of microwave stepped-impedance resonators," *IEEE Transactions on Mirowave Theory*, vol. 45, no. 7, pp. 1078-1084, 1997.

[18] R. Dhakal and N. Kim, "A compact symmetric microstrip filter based on a rectangular meandered-line stepped impedance resonator with a triple-bandstop ronespse," *The Scientific World Journal*, vol. 2013, pp. 1-7, 2013

[19] H. Zhang and K. Chen, "Miniaturized coplanar waveguide bandpass filters using multisection stepped-impedance resonators," *IEEE Transactions on Mirowave Theory*, vol. 54, no. 3, pp. 1090-1095, 2006.

[20] R. Simons, *Coplanar Waveguid Circuits, Components And Systems*, John Wiley and Sons, 2001.

[21] S. Alja'afreh, Y. Huang, L. Xing, Q. Xu, and X. Zhu, "A low profile and wideband PILA-based antenna for handset diversity applications," *IEEE Antenna Wireless Propagation Letter*, vol. 14, pp. 923-926, 2015.

[22] T. Nakamura, M. Shimizu, H. Kimura, and R. Sato, "Effective permittivity of amorphous mixed materials," *Electronics and Communications in Japan*, vol. 88, no. 10, 2005.

[23] R. Simons, *Coplanar Waveguide Circuits, Components and Systems*, John Wiley and Sons, 2001.

[24] R. Vaughan and J. Andersen, "Antenna diversity in mobile communications," *IEEE Transactions on Vehicular Technology*, vol. 36, no. 4, pp. 149-172, 1987.

[25] S. Blanch, J. Romeu, and I. Corbella, "Exact representation of antenna system diversity performance from input parameter description," *Electronics Letters*, vol. 39, no. 9, pp. 705-707, 2003.

[26] P. Hallbjorner, "The significance of radiation effeciencies when using S-parameters to calculate the received signal correlation from two antennas," *IEEE Antenna Wireless Propagation Letter*, vol. 4, pp. 97-100, 2005.

[27] T. Taga, "Analysis for mean effective gain of mobile antennas in land mobile radio environments," *IEEE Transactions on Vehicular Technology*, vol. 39, no. 2, pp. 117-131, 1990.

[28] S. Ko and R. Murch, "Compact integrated diversity antenna for wireless communications," *IEEE Transactions on Antennas and Propagation*, vol. 49, no. 6, pp. 954-960, 2001.

[29] M. Karaboikis, V. Papamichael, and G. Tsachtsiris, "Integrating compact printed antenna onto small diversity/MIMO terminal," *IEEE Transactions on Antennas and Propagation*, vol. 56, no. 7, pp. 2067-2078, 2008.

[30] V. Plicanic, "Antenna diversity studies and evaluation," *M.Sc. Thesis,* Lund University, May. 2004 [Online]. Avialable: htttp:// www,es.lth.se/teorel/publications/TEAT-500-se-ries/TEAT-5064.pdf.

[31] S. Alja'afreh, Y. Huang, and L. Xing, "Compact, wideband and low profile planar inverted-L antenna," *Proceedings of the European Conference on Antenna and Propagation*, pp. 3283-3286, 2014.

[32] C. Holloway, H. Shah, R. Pirkl, W. Young, D. Hill, and J. Ladbury, "Reverbration chamber techniques for determining the radiation and total efficiency of antennas," *IEEE Transactions on Antennas and Propagation*, vol. 60, no. 4, pp. 1758-1770, 2012.

[33] K. Rosengren and P. Kildal, "Radiation efficiency, correlation, diversity gain and capacity of a six-monopole antenna array for a MIMO system: theory, simulation and measurement in reverberation chamber," *IEE Proceedings, Microwaves, Antennas and Propagation*, vol. 152, no. 1, pp. 7-16, 2005.